Brownian rod-like particles suspension in non-homogeneous system: flow-microstructure coupling

Hamza Issa, Giovanniantonio Natale, Gilles Ausias, Julien Férec

Brownian rod-like particles suspension in non-homogeneous system: flow-microstructure coupling

Hamza Issa
Univ. Bretagne Sud, UMR CNRS 6027, IRDL, F-56100 Lorient, France
Department of Chemical and Petroleum Engineering, Schulich School of Engineering, University of Calgary, 2500 University Drive NW, T2N 1N4, Canada

Giovanniantonio Natale
Department of Chemical and Petroleum Engineering, Schulich School of Engineering, University of Calgary, 2500 University Dr. NW, T2N 1N4, Canada[*]

Gilles Ausias
Univ. Bretagne Sud, UMR CNRS 6027, IRDL, F-56100 Lorient, France

Julien Férec
Univ. Bretagne Sud, UMR CNRS 6027, IRDL, F-56100 Lorient, France [†]
(Dated: November 25, 2024)

This study investigates the microstructure and rheological response of Brownian rod suspensions considering both spatial and orientational fluctuations in simple shear, Poiseuille and Couette flows. Focusing on rod-fluid interactions and concentration gradients, we account here for the effects of the rods concentration-orientation coupling. Numerical simulations, based on a kinetic macro-model previously derived [1], are used to analyze these results. In simple shear flow, the presence of the rods do not impact the flow, and translational diffusion does not modify the rheological properties of the suspensions. In Poiseuille flow, the rods cause a flattening of the velocity profile and the two-way coupling enhances the cross-streamlines migration toward the walls. The two-way coupling between the flow field and the rods control their orientation, migration behavior, and rheological properties. In Couette flow, rod-fluid coupling results in outward flow near the fixed cylinder. The translational diffusion plays a crucial role as higher translational Peclet numbers lead to pronounced migration of rods towards the channel walls and increased alignment in the flow direction. This coupling effect also affects the velocity profile in Couette flow. Our findings provide valuable insights into the complex behavior of suspended Brownian rods in different flow conditions.

I. INTRODUCTION

In material engineering, predicting and controlling the local configuration state of particle suspensions (i.e., spatial and orientational distribution) is critical to design advanced manufacturing processes [2–4]. Modelling of such processes in the case of colloidal suspensions is a difficult undertaking. It requires resolving particle-particle interactions, thermal fluctuations, and long-range many-body hydrodynamic interactions that lead to complex suspension microstructures and rheological responses [5, 6]. Researchers have theoretically and numerically studied the evolution of the orientation of anisometric particles homogeneously suspended during flow. In what follows, we organize the findings based on linear and non-linear flows.

In linear flows, Jeffery [7] derived the equation of motion for a single isolated, inertialess, ellipsoidal, non-Brownian particle in a Newtonian fluid. When a dilute slender fiber suspension is subjected to constant shear flow, particles orient in the flow direction and spent most of their time aligned in this latter direction [8, 9]. For many Brownian particles, a statistical description is required. Doi and Edwards [10] obtained a Fokker-Planck equation for Brownian rigid rods, where the orientation convective flux is provided by the Jeffrey's result. Dhont and Briels [11] derived the Doi-Edwards framework from first principles explicitly accounting for the rod dynamical correlations. Férec et al. [12], and later, Natale et al. [13] developed a new set of constitutive equations accounting for a linear and non-linear lubrication interaction, respectively, between rods dispersed in a Newtonian matrix. Natale et al. [13] showed that the non-linear lubrication interaction was sufficient to predict the shear-thinning behavior of attractive Brownian rod suspensions. Hinch and Leal [14] revealed the intricate interplay between shear flow alignment and Brownian disorientations in a dilute suspension of axisymmetric particles. The rheological behavior exhibits oscillatory features

[*] gnatale@ucalgary.ca
[†] julien.ferec@univ-ubs.fr

tied to particle rotation and a fading memory effect due to Brownian diffusion. Hijazi and Zoaeter [15] used Brownian dynamics simulations to study rod-like particles in a dilute flowing solution. Their results demonstrated the impact of the hydrodynamic shear rate and rotational Brownian diffusion on the average orientations, with the maximum orientation angle exhibiting a strong dependence on the flow conditions. Leahy et al. [16] examined the effect of shear flow on the rotational diffusion of a single axisymmetric particle. Their study provided new insights into the time-dependent rheological properties of suspensions containing non-spherical Brownian particles. They found two distinct diffusive time scales in the rheology that scale separately with aspect ratio. The study highlights the complex interplay between shear-induced rotations and diffusion, revealing the importance of particle shape and orientation dynamics in determining the behavior and properties of such suspensions. Palanisamy and den Otter [17] developed an efficient Brownian dynamics simulation method for rigid colloids in linear flow fields based on the grand mobility matrix. This study on suspensions of non-spherical Brownian particles revealed that the rheological properties in continuous shear flow are influenced by two distinct diffusive time scales, which depend on the particle aspect ratio.

In non-linear flows, Schiek and Shaqfeh [18] studied theoretically the cross-streamline migration of slender Brownian rods in plane Poiseuille flow. It provides insights into the occurrence of migration and the distribution patterns of particles on scales comparable to the particle length within the channel, where rods migrate away from the center of the channel and towards the channel walls. Nitsche and Hinch [19] investigated the shear-induced lateral migration of Brownian rigid rods in parabolic channel flow and quantitatively confirmed the accumulation of rods at the channel walls. Xie et al. [20] used experimental techniques to study the shear-induced alignment of low aspect ratio gold nanorods in Newtonian fluids. Their observations highlight the alignment phenomenon and numerical simulations support the understanding of the nanorods behavior, including the impact of Brownian motion even at high Peclet numbers. Numerical simulations show that the rods flipping between extreme orientations of the Jeffery's orbits and that the effect of the Brownian motion on the gold nanorods cannot be ignored even at large Péclet number. Kumar and Natale [21] investigated the settling dynamics of two spheres in a suspension of Brownian rods using numerical simulations. They found that the presence of Brownian rods introduces non-Newtonian contributions, resulting in repulsive interactions between the settling spheres that depend on the Peclet number and the distance between their centers.

Fokker-Planck-like equations in multiple dimensions are computationally expensive to solve. The creation of an equivalent kinetic macro-model is a tactic used to make the numerical solution of complex physics problems more accessible. Macro models have been used extensively in the literature to forecast particle concentration or orientation. To describe fiber orientation in suspensions containing short rigid fibers, Advani and Tucker [22] used a set of even-order moments of the probability distribution function. In concentrated, monomodal, spherical suspensions, Phillips et al. [23] proposed a constitutive equation for computing particle concentration and velocity fields. Shapley et al. [24] compared the predictions of various particle migration models to laser Doppler velocimetry measurements. At moderate bulk particle concentrations, the models accurately predict the macroscopic shear rate and concentration profiles, but at high concentrations, they start to diverge. Without considering the correlation between the two, these models are either used to predict the orientation or the concentration. Férec et al. [25] examined the Folgar-Tucker-Lipscomb model without any closure approximation. They discussed the accuracy of commonly used closure approximations. As per extant literature, the Invariant-based optimal fitting (IBOF) proposed by Chung et al. [26] stands out as the most precise closure approximation available. Saintillan and Shelley [27] developed a kinetic model and discussed the stability and non-linear dynamics of a suspension of self-propelled rod-like particles. For an active suspension, Weady et al. [28] restated and coarse-grained a continuum kinetic model. Although the translational diffusion is anisotropic and depends on the particle's orientation, these two models assume it as a constant. Issa et al. [1] derived a new kinetic macro-model based on moments of the probability distribution function to investigate the flow of Brownian particle suspensions taking into account the anisotropic translational diffusion. The rod migrations across the flow streamlines were caused by Brownian translational Peclet numbers but particle-induced stresses were neglected.

Many studies have studied the two-way coupling, which refers to the mutual influence between the fluid flow and the suspended particles, In a series of influential papers [29–31], Batchelor and coworkers established that microstructural asymmetry, not just distortion, is required to produce non–Newtonian rheology. They established expressions for the average suspension stress in dilute colloidal dispersion, as well as the non-equilibrium Smoluchowski framework that governs the evolution of a flowing microstructure under the influence of thermodynamic and hydrodynamic forces. Several studies have confirmed that particles alter the flow pattern of suspensions. Bagnold [32] reported the appearance of normal stresses during shear flow on flow-induced non-Newtonian rheology of suspensions of non-colloidal spherical particles. He proposed that non-Newtonian rheology was caused by the presence of a particle microstructure and shear-flow-induced changes in its shape. The existence of a shear-induced structure in concentrated non-colloidal suspensions was conclusively suggested by several studies after this innovative work [33, 34]. Mezi et al. [35] developed a numerical simulation for 2D planar flows for fiber suspension with a Newtonian and a power-law suspending fluids. Then, they extended this model to examine a 2D axisymmetric capillary die swell for fiber

suspensions, which occurs in 3D printing extrusion processes [36]. The particle extra stress flattens the velocity profile but has little effect on the distribution of fiber orientation in the suspension during flow. Yasuda et al. [37] measured the velocity profile of short fibers in a Newtonian matrix flow inside a channel with a rectangular cross-section. They observed that the velocity profile becomes flatter as the fiber volume fraction increases. Mazahir et al. [38, 39] used slow orientation kinetics such as the reduced strain closure model [40] to conduct coupled transient simulations to predict fiber orientation in a center-gated disc. They discovered that the numerical data of the coupling effect is very small when compared to experimental data measured in the shell, transition, and core layers, but there is an improvement in the frontal flow region. A two-way coupled direct simulation technique is proposed by Moosaie and Manhart [41] for the numerical solution of Brownian rod suspension flows in complex geometries. They observed that, in the case of channel flow, the bulk velocity in the channel decreases by the effect of extra stress generated by the rods. Krochak et al. [42] examined the effect of two-way coupling between the flow field and the orientation state of rigid fiber suspensions flowing through a tapered channel with an orientation distribution function that evolves according to a Fokker-Planck-type equation. When the two-way coupling was taken into account, it was demonstrated that the suspension aligned much more quickly, and the orientation anisotropy profiles differed significantly.

We end this section by reporting a sentence that has puzzled generations of rheologists and soft-matter physicists and motivated us to explore the effects of an anisotropic translational diffusion tensor. In the renowned book 'The Theory of Polymer Dynamics', Doi and Edwards [10] pointed out in chapter 8 that "..., a concentration gradient of rodlike polymer can induce an anisotropy in the orientational distribution. However, the reverse is not true: in a homogeneous system (in which the positional distribution is uniform), the translation-rotation coupling has no effect: if the system is homogeneous, it will remain homogeneous even if the orientational distribution is not isotropic." We will show in the following that this statement is only valid in the case of simple shear flow. Therefore, the objective of this work is to investigate the effect of flow/Brownian rod microstructure coupling in non-homogeneous systems while considering the evolution of the particle concentration and orientation. The study employs a kinetic macro-model derived in a previous work [1] and examines particle suspensions in a planar infinite channel and couette flow between two cylinders during transient studies. The article is organized as follows: Section II focuses on the flow problem and theoretical modeling for Brownian rod suspensions. Finally, Section III presents the numerical results, including the effect of particle extra stresses, the effect of translational diffusion, and the effect of both initial concentration and orientation gradients, before the conclusion.

II. GOVERNING EQUATIONS

Let's consider a suspension of Brownian rod-like particles of length L, circular cross-section of diameter D, and an aspect ratio $a_r = L/D$. The particles are assumed to be rigid, monodisperse, neutrally buoyant, and immersed in a Newtonian fluid. The rod suspension is supposed to be diluted in a volume of interest V. Hence the mean number of rods per unit volume n verified that $nL^3 << 1$. The fluid is presumed to be isothermal and incompressible. Below are presented the equations that describe the flow problem and the kinetic macro-model of the suspending rods. Subsequently, these equations are written in dimensionless form for further analysis and simplification.

A. Flow problem

The problem is governed by the continuity and Cauchy momentum equations in the limit of creeping flow (low Reynolds number)

$$\nabla_{\mathbf{x}} \cdot \mathbf{u} = 0, \tag{1}$$

$$\nabla_{\mathbf{x}} P - \eta_0 \nabla^2_{\mathbf{x}} \mathbf{u} = \nabla_{\mathbf{x}} \cdot \mathbf{\Sigma}. \tag{2}$$

In the above equations, $\nabla_{\mathbf{x}}$ and $\nabla^2_{\mathbf{x}}$ are the gradient and Laplacian operators in the spatial space, respectively. $\mathbf{u}$ is the velocity vector of the suspension, P denotes the pressure, η_0 is the Newtonian dynamic viscosity of the suspending fluid and $\mathbf{\Sigma}$ represents the particle extra stress tensor. Indeed, the presence of particles in a Newtonian medium develops extra stress contributions, which are obtained by configurational averages of force dipoles exerted by the particle on the fluid. In a dilute regime, the particle extra stress tensor arises from two contributions [27]

$$\mathbf{\Sigma} = \mathbf{\Sigma}_B + \mathbf{\Sigma}_F. \tag{3}$$

The first contribution is because particles are Brownian

$$\boldsymbol{\Sigma}_B = k_B T(3\mathbf{A}_2 - \mathbf{A}_2 : \boldsymbol{\delta}\boldsymbol{\delta}), \tag{4}$$

where k_B and T are the Boltzmann constant and the absolute temperature, respectively, and $\boldsymbol{\delta}$ is the identity tensor. The second contribution comes from the inextensibility condition of the particles and is expressed as

$$\boldsymbol{\Sigma}_F = \sigma_F \left[\left(\mathbf{A}_4 - \frac{1}{3}\boldsymbol{\delta}\mathbf{A}_2 \right) : \dot{\boldsymbol{\gamma}} \right], \tag{5}$$

where $\sigma_F = \pi\eta_0 L^3/6\log(2a_r)$ from slender body theory, and $\dot{\boldsymbol{\gamma}}$ is the strain-rate tensor. $\mathbf{A}_2$ and $\mathbf{A}_4$, which will be defined below, represent the second and fourth-order conformation tensors, respectively.

B. Kinetic model

In a local volume, which is large enough to contain a statistically significant number of particles but smaller than the characteristic length scale of the macroscopic properties of the system under consideration, a Brownian particle suspension can be characterized by a distribution function $\Psi(\mathbf{x}, \mathbf{p}, t)$. It reflects the probability of finding a particle at position $\mathbf{x}$ with orientation $\mathbf{p}$, at time t. Therefore, $\Psi(\mathbf{x}, \mathbf{p}, t)d\mathbf{x}d\mathbf{p}$ represents the number of particles with center of mass and orientation vectors in a range $d\mathbf{x}d\mathbf{p}$ about $\mathbf{x}$ and $\mathbf{p}$ at the current time t. A single particle Smoluchowski equation can be obtained in the dilute regime as follows [10, 35]

$$\frac{\partial \Psi}{\partial t} = -\nabla_{\mathbf{x}} \cdot (\dot{\mathbf{x}}\Psi) - \nabla_{\mathbf{p}} \cdot (\dot{\mathbf{p}}\Psi), \tag{6}$$

where $\nabla_{\mathbf{p}}$ is the gradient operator in the configurational space. The time-dependent evolution of the position of a Brownian particle, $\dot{\mathbf{x}}$, is

$$\dot{\mathbf{x}} = \mathbf{u} - \mathbf{D}_t \cdot \nabla_{\mathbf{x}} \log \Psi, \tag{7}$$

and the time-dependent evolution of its orientation, $\dot{\mathbf{p}}$, can be written as

$$\dot{\mathbf{p}} = \dot{\mathbf{p}}_j - D_r \nabla_{\mathbf{p}} \log \Psi, \tag{8}$$

where $\dot{\mathbf{p}}_j$ is the Jeffery's equation such as

$$\dot{\mathbf{p}}_j = -\frac{1}{2}\boldsymbol{\omega} \cdot \mathbf{p} + \frac{\lambda}{2}(\dot{\boldsymbol{\gamma}} \cdot \mathbf{p} - \dot{\boldsymbol{\gamma}} : \mathbf{ppp}). \tag{9}$$

The rotational diffusion coefficient and translational diffusion tensor are denoted by D_r and $\mathbf{D}_t$, respectively. The latter is defined for non-spherical, rigid particles as $\mathbf{D}_t = D_{\parallel}\mathbf{pp} + D_{\perp}(\boldsymbol{\delta} - \mathbf{pp})$, where $D_{\parallel}$ and $D_{\perp}$ are constants that characterize the diffusion parallel and perpendicular to the particle axis, respectively. The vorticity tensor is denoted by $\boldsymbol{\omega}$ and λ is a constant shape factor as a function of the rod aspect ratio a_r. The combination of the above equations, with the help of the continuity equation, leads to

$$\frac{D\Psi}{Dt} = \nabla_{\mathbf{x}} \cdot (\mathbf{D}_t \cdot \nabla_{\mathbf{x}}\Psi) - \nabla_{\mathbf{p}} \cdot (\dot{\mathbf{p}}_j\Psi) + D_r \nabla_{\mathbf{p}}^2 \Psi, \tag{10}$$

where $D(...)/Dt = \partial(...)/\partial t + \mathbf{u} \cdot \nabla_{\mathbf{x}}(...)$ is the material derivative. Based on the distribution function, its moments can be written. Specifically, the fourth-order, the second-order, and the zeroth-order moments of Ψ are respectively defined as [1]

$$\mathbf{A}_4 = \int_{\mathbf{p}} \mathbf{pppp}\Psi d\mathbf{p}, \tag{11}$$

$$\mathbf{A}_2 = \mathbf{A}_4 : \boldsymbol{\delta} = \int_{\mathbf{p}} \mathbf{pp}\Psi d\mathbf{p}, \tag{12}$$

$$c = \mathbf{A}_2 : \boldsymbol{\delta} = \int_{\mathbf{p}} \Psi d\mathbf{p}, \tag{13}$$

where c represents to the local number density of the suspension, which is directly linked to the trace of $\mathbf{A}_2$. The moments $\mathbf{A}_4$ and $\mathbf{A}_2$ contain information on the local concentration and orientation of particles. For instance, a local population of rods oriented randomly with a number density c_1 is given by $\mathbf{A}_2 = c_1\boldsymbol{\delta}/3$, whereas a group of rods having the same direction with a number density c_2 leads that $\mathbf{A}_2$ has only one non-zero component in the alignment direction equals to c_2. Therefore, it is found that the distribution function Ψ is normalized such as

$$\frac{1}{V}\int_{\mathbf{x}}\int_{\mathbf{p}} \Psi d\mathbf{p}d\mathbf{x} = n. \tag{14}$$

After some straightforward algebraic manipulations, an evolution equation of the tensor $\mathbf{A}_2$ can be derived [1]

$$\begin{aligned}\frac{D\mathbf{A}_2}{Dt} =& -\frac{1}{2}\left(\boldsymbol{\omega}\cdot\mathbf{A}_2 - \mathbf{A}_2\cdot\boldsymbol{\omega}\right) + \frac{\lambda}{2}\left(\dot{\boldsymbol{\gamma}}\cdot\mathbf{A}_2 + \mathbf{A}_2\cdot\dot{\boldsymbol{\gamma}} - 2\mathbf{A}_4 : \dot{\boldsymbol{\gamma}}\right) + 2D_r\left(c\boldsymbol{\delta} - 3\mathbf{A}_2\right) \\ &+ D_\perp\nabla^2_{\mathbf{x}}\mathbf{A}_2 + \left(D_\parallel - D_\perp\right)\nabla_{\mathbf{x}}\nabla_{\mathbf{x}} : \mathbf{A}_4.\end{aligned} \tag{15}$$

Since Eq. (15) involves $\mathbf{A}_4$, it requires a closure approximation to express $\mathbf{A}_4$ in terms of $\mathbf{A}_2$. Fortunately, standard closure approximations [26, 43, 44] can be used for this case, by being cautious to normalise $\mathbf{A}_2$ by c in order to maintain the unitary trace condition. In our previous investigation [1], the IBOF closure [26] was tested and yielded more than 95% accurate results as compared to the exact solution obtained by solving the Fokker-Planck equation given by Eq. (10). Hence, all the cases presented in this work involved the IBOF closure for the analysis. Eq. (15), called macro-model, allows for solving of a set of partial differential equations (i.e., 6 PDEs in 3D, which are the evolution of A_{11}, A_{22}, A_{33}, A_{12}, A_{13} and A_{23}) rather than a full 6D Fokker-Planck equation (i.e., 3D in spatial space, 2D in configurational space and 1D in time), greatly simplifying the numerical simulation.

C. Dimensionless formulation of the problem

To render the problem dimensionless, the particle length L and the Newtonian viscosity of the suspending fluid η_0 are chosen as the characteristic length and viscosity, respectively. Therefore, the characteristic strain rate is $\dot{\gamma} = U_{avg}/L$, where U_{avg} is the average flow velocity. We also introduce a dimensionless mean number density such as $c^* = c/n$, where n is the mean number density. The dimensionless form of the Cauchy equation can be written as

$$\nabla^*_{\mathbf{x}}P^* - \nabla^{*2}_{\mathbf{x}}\mathbf{u}^* = \nabla^*_{\mathbf{x}}\cdot\left\{c^*\left[N_p\left(\mathbf{A}^*_4 - \frac{1}{3}\boldsymbol{\delta}\mathbf{A}^*_2\right) : \dot{\boldsymbol{\gamma}}^* + N_b\left(3\mathbf{A}^*_2 - \boldsymbol{\delta}\right)\right]\right\}. \tag{16}$$

As a result, the dimensionless form of the stress tensor is

$$\boldsymbol{\Sigma}^* = c^*\left[N_p\left(\mathbf{A}^*_4 - \frac{1}{3}\boldsymbol{\delta}\mathbf{A}^*_2\right) : \dot{\boldsymbol{\gamma}}^* + N_b\left(3\mathbf{A}^*_2 - \boldsymbol{\delta}\right)\right], \tag{17}$$

where $N_p = \frac{\pi n L^3}{6log(a_r)}$ is the particle coupling coefficient, and $N_b = \frac{nk_BT}{\eta_0\dot{\gamma}}$ is the Brownian coupling coefficient. Following the previous work [1], $Pe_r = \dot{\gamma}/D_r$, $Pe_\perp = L^2\dot{\gamma}/D_\perp$ and $Pe_\parallel = L^2\dot{\gamma}/D_\parallel$ are the rotary, perpendicular and parallel Peclet numbers, respectively. For very long and thin rod-like particles, $\lambda = 1$ and the relation $Pe_\perp = 2Pe_\parallel$ applies [10]. Based on this, the evolution equation for $\mathbf{A}_2$ in dimensionless form becomes

$$\begin{aligned}\frac{D\mathbf{A}^*_2}{Dt^*} =& -\frac{1}{2}\left(\boldsymbol{\omega}^*\cdot\mathbf{A}^*_2 - \mathbf{A}^*_2\cdot\boldsymbol{\omega}^*\right) + \frac{1}{2}(\dot{\boldsymbol{\gamma}}^*\cdot\mathbf{A}^*_2 + \mathbf{A}^*_2\cdot\dot{\boldsymbol{\gamma}}^* - 2\mathbf{A}^*_4 : \dot{\boldsymbol{\gamma}}^*) + \frac{2}{Pe_r}\left(\boldsymbol{\delta} - 3\mathbf{A}^*_2\right) \\ &+ \frac{1}{Pe_\perp}\nabla^{*2}_{\mathbf{x}}\mathbf{A}^*_2 + \frac{1}{Pe_\perp}\nabla^*_{\mathbf{x}}\nabla^*_{\mathbf{x}} : \mathbf{A}^*_4,\end{aligned} \tag{18}$$

where $t^* = t\dot{\gamma}$. The evolution equation of concentration c^* is simply obtained by taking the trace of the above equation

$$\frac{Dc^*}{Dt^*} = \frac{D\mathbf{A}_2^*}{Dt^*} : \boldsymbol{\delta} = \frac{1}{Pe_\perp}\nabla_{\mathbf{x}}^{*2}c^* + \frac{1}{Pe_\perp}\nabla_{\mathbf{x}}^*\nabla_{\mathbf{x}}^* : \mathbf{A}_2^*. \tag{19}$$

Eqs. (18) and (19) show the coupling between the concentration and the local orientation of the Brownian rods. This coupling clearly appears in the last term of Eq. (19). In what follows the asterisks indicating the non-dimensional quantities have been dropped for clarity.

III. NUMERICAL RESULTS

In this work, three shear flow problems (simple shear flow, Poiseuille flow and Couette flow) are tested using the kinetic macro-model with the IBOF closure, which corresponds in solving Eqs. (1), (2) and (18) in their dimensionless form. The accuracy of this model has been verified in Appendix A with comparing the results with the solution of the full Fokker-Planck equation for simple shear flow (uncoupled model). The dimensionless shear viscosity is given by $\eta = \Sigma_{12}$ and the dimensionless first and second normal stress differences N_1 and N_2 are $N_1 = \Sigma_{11} - \Sigma_{22}$ and $N_2 = \Sigma_{22} - \Sigma_{33}$, respectively. Actually, the indices 1, 2 and 3 denote the flow direction, the velocity gradient direction and the vorticity direction, respectively. Therefore, in a simple shear flow and Poiseuille flow, they correspond to x, y and z, respectively, while in the Couette flow, they refer to θ, r and z, respectively. Initial conditions (unless otherwise mentioned) are $\mathbf{A}_2 = \boldsymbol{\delta}/3$ and $c = 1$. It means that particles have a 3D random orientation with no concentration gradient.

A. Simple shear flow

First, we consider a suspension flowing between two moving parallel plates. The geometry is a 2D square channel of side H, where $H/L = 10^6$. A simple shear flow is imposed in the xy-plane, where the upper wall at $y = H/2$ translates at $\dot{\gamma}H/2 = 0.5$ in the x-direction, whereas the lower wall at $y = -H/2$ translates in the opposite direction. Due to the symmetric conditions along the $y = 0$ axis, all results in the rectangular channel are plotted for $0 < y/H < 0.5$. Periodic flow conditions with $\Delta P = 0$ at ($x = 0$ and $x = H$) are used to simulate the flow in an infinite channel.

1. Homogeneous systems

Under the one-way coupling assumption ($N_p = 0$ and $N_b = 0$), we first explore the flow-induced microstructure change for a homogeneous system in a simple shear flow. Numerical simulations are performed for $Pe_\perp = 0.01, 0.1, 1$ and 10, with a fixed value of $Pe_r = 10$. There is no effect of translational diffusion on the system. No effect on the rod orientation dynamics, shear viscosity, and normal stress differences is observed and no rod migration occur (results not shown). This is confirmed by the fact that the right-hand side of Eq. (19) is always null. We then examine the flow-microstructure coupling for $N_b = 0, 10, 100, 250$ and 1000 and $N_p = 0, 10, 100$ with $Pe_\perp = Pe_r = 10$. The two-way coupling does not change the velocity profile in simple shear flows (as expected for viscometric flows) and does not modify the rod orientations as well as the rheological properties (shear viscosity and normal stress differences).

2. Non-homogeneous systems - Effect of concentration gradient

We now investigate the effect of various initial concentrations on the transient rheological properties of Brownian rod suspensions. As depicted in Fig. 1, six initial concentration gradient cases along the y-direction are examined with the following equations, $c_1 = 1$, $c_2 = -2.57y^2 + 1.21$, $c_3 = -3.43y^2 + 1.28$, $c_4 = -5.14y^2 + 1.42$, $c_5 = 1.42$ for $0 < y < 0.35$ else $c_5 = 0.0014$ and $c_6 = 2.856$ for $0 < y < 0.1755$ else $c_6 = 0.0014$. The average concentration in the channel is kept constant to 1 for all the cases. Particles are initially isotropically oriented. The two-way coupling assumption is taken into consideration. To examine the impact of concentration, it is necessary to keep the other parameters influencing the study constant, such as maintaining fixed values for $N_b = 250$, $N_p = 10$, and $Pe_r = Pe_\perp = 10$. In these cases, the presence of an initial concentration gradient results in a non-uniform distribution of particles within the channel. As a result, particle migration occurs across the streamlines due to translational diffusion. The presence of a concentration gradient in the y-direction leads to the right-hand side term in Eq. (19) becoming non-zero, which

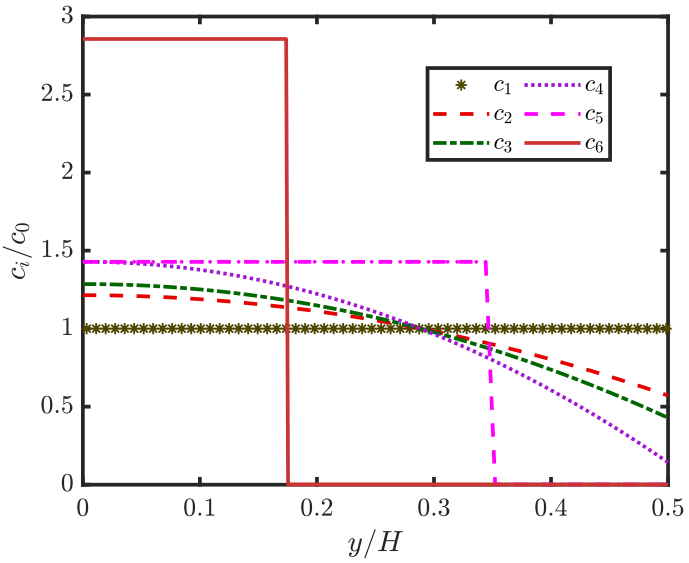

FIG. 1: Initial concentration gradients $c_1 = 1$, $c_2 = -2.57y^2 + 1.21$, $c_3 = -3.43y^2 + 1.28$, $c_4 = -5.14y^2 + 1.42$, $c_5 = 1.42$ for $0 < y < 0.35$ else $c_5 = 0.0014$ and $c_6 = 2.856$ for $0 < y < 0.1755$ else $c_6 = 0.0014$.

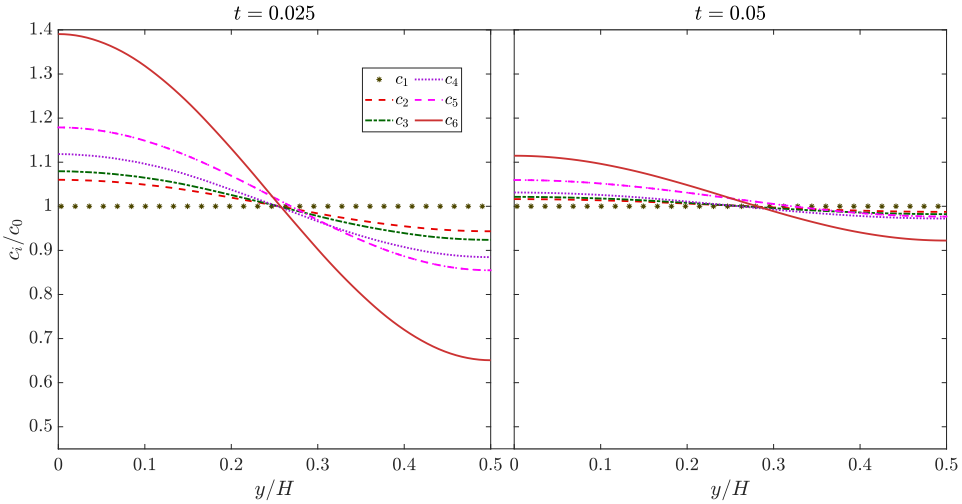

FIG. 2: Evolution of concentration distribution along the y-direction for various initial concentration gradients at $t = 0.025$ and 0.05.

subsequently induces particle migrations. Indeed, since t increases, the concentration gradient gradually changes as reported in Fig. 2, until reaching a uniform concentration distribution $c_i = 1$ at the steady state ($t \approx 0.2$). However, in these cases, it is worth mentioning that the migration of rods does not have an impact on their orientation dynamics. As a result, the transient rheological properties, which are specifically related to the orientation distributions of the rods, remain unaffected by rod migrations.

3. Non-homogeneous systems - Effect of orientation gradient

To explore the influence of orientation along the y-direction, an orientation gradient is imposed in a simple shear flow keeping the concentration constant and homogeneous. Four initial orientation gradient cases are examined, as shown in Fig. 3, for which $A_{yy} = A_{zz}$ and $A_{xy} = 0$. The first case is referred to as "ISO", where the rod orientation is isotropic, i.e., $\mathbf{A}_2 = \boldsymbol{\delta}/3$. In the second case called "ALI", particles are perfectly aligned in the flow direction (i.e.,

$A_{xx} = 1$). "LIN" corresponds to the initial condition, where the orientation gradient has a linear profile. $A_{xx} = 1$ and $A_{yy} = 0$ at the walls ($y = 0.5$), whereas $A_{xx} = 0$ and $A_{yy} = 0.5$ at center-line ($y = 0$). The latest case denoted "QUA" considers a quadratic form for the orientation gradient, where rods are aligned in the flow direction at the center-line, $A_{xx} = 1$ and $A_{yy} = 0$, while at walls ($y = 0.5$), $A_{xx} = 0$ and $A_{yy} = 0.5$. To isolate the effect of orientation, parameters are fixed to $N_b = 250$, $N_p = 10$, and $Pe_\perp = Pe_r = 10$. No cross-streamline migrations of the rods are observed. Furthermore, the various initial orientations of rods do not modify their final orientation distributions and consequently the final rheological properties of the system. However, it changes the transient rheological properties of the system.

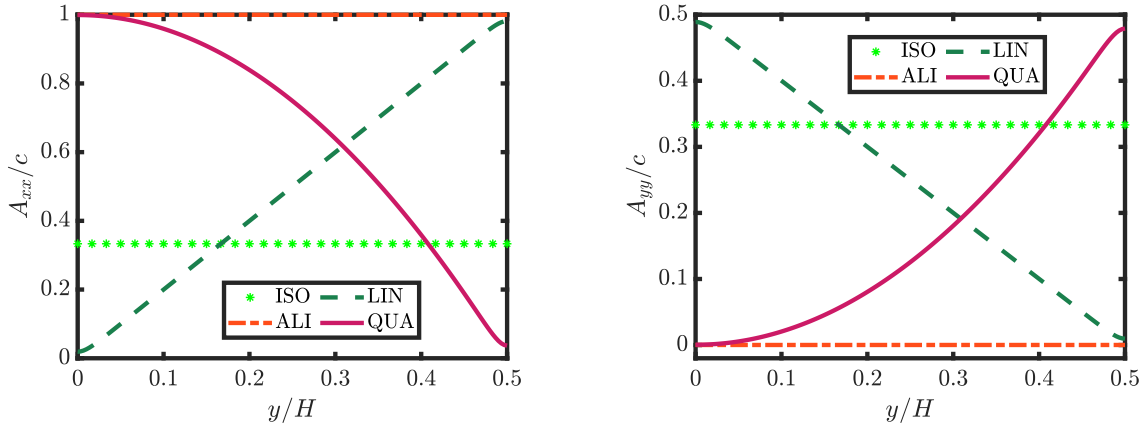

(a) Initial distribution of A_{xx} along the y-direction. (b) Initial distribution of A_{yy} along the y-direction.

FIG. 3: Initial rod orientations, "ISO", "LIN", "ALI", and "QUA" for (a) A_{xx} and (b)A_{yy} in the y-direction.

Evaluated at $x = 0$, Fig. 4, 5, and 6 depict the time evolution along the y-direction for Σ_{xy}, N_1 and N_2, respectively. These figures provide valuable information about how the rheological properties of the system evolve over time in response to changes in the initial orientation of the rods. The study reveals that rheological properties are strongly linked with rod orientation distributions.

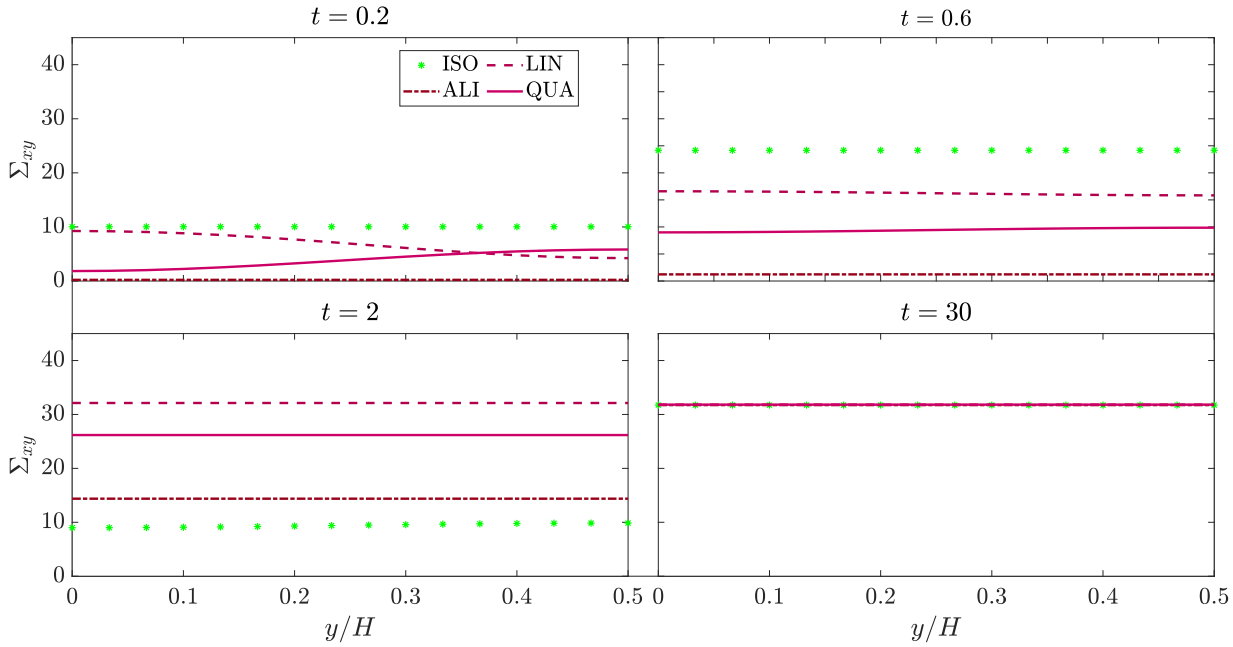

FIG. 4: Evolution of the shear stress along the y-direction for various initial rod orientations at $t = 0.2, 0.6, 2$ and 30.

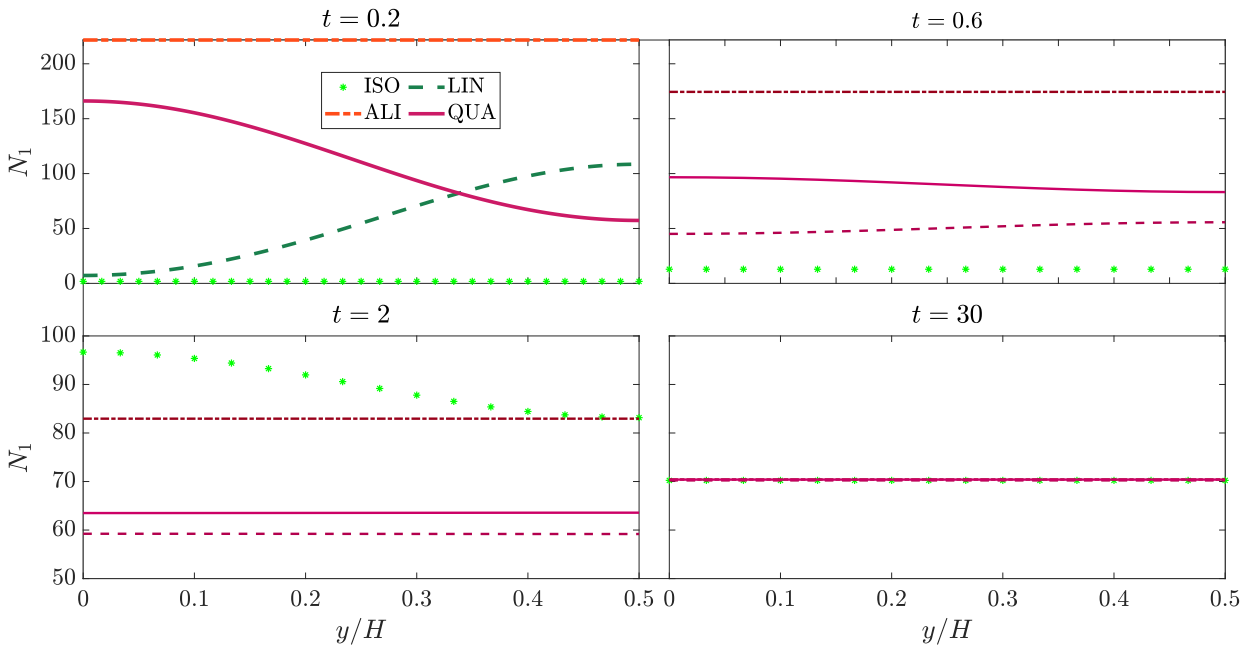

FIG. 5: Evolution of the first normal stress difference along the y-direction for various initial rod orientations at $t = 0.2, 0.6, 2$ and 30.

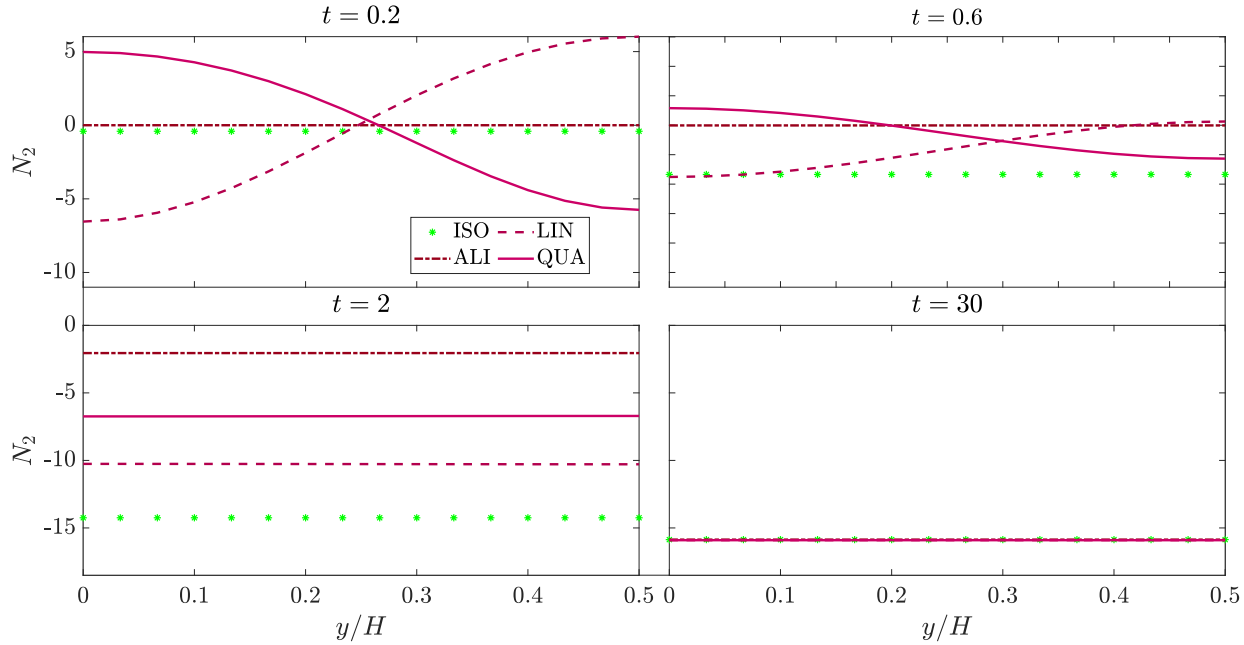

FIG. 6: Evolution of the second normal stress difference along the y-direction for various initial rod orientations at $t = 0.2, 0.6, 2$ and 30.

B. Poiseuille flow

Let's consider now the planar Poiseuille flow problem. The geometry consists of a 2D square of side H and, therefore, the flow occurs in the xy-plane (x being the flow direction and y the velocity gradient direction). The two fixed walls are located at $y \pm 1/2$. Periodic flow conditions of constant flow rate are used to simulate an infinite flow in the

channel. The prescribed initial condition for the velocity is parabolic with $u_x = 1 - 4y^2$ and $u_y = 0$.

1. *Effect of particle extra stress*

By taking into account the two-way coupling effects in homogeneous systems, it is known that the presence of particles in the fluid causes a flattening of the standard parabolic velocity profile in a Poiseuille flow [36]. However, in our study, we focus on non-homogeneous systems, where migrating rods lead to the formation of concentration variations, thus deviating from homogeneity. Hence, to investigate the impact of particle extra stress on the system, we keep constant the translational and rotational Peclet numbers at a value of 10 (i.e., $Pe_r = Pe_\perp = 10$). This allows us to isolate and analyze the specific influence of the additional stress on the system (i.e., the effect of the coupling).

Fig. 7a presents the numerical results obtained by investigating the coupled flow field and rod conformations, in particular the effect of Brownian stress contribution through N_b. Starting from a prescribed parabolic velocity profile with an isotropic orientation distribution and $c(t = 0) = 1$, the velocity profile tends to flatten out with time (results not shown). The system is fully developed at $t = 30$. As increasing N_b, the velocity profile tends to flatten more. For $N_b = 10$, the effect on the velocity profile is relatively small. However, as N_b increases, particle stresses increase leading to a more significant deviation from the standard parabolic profile.

Fig. 7b depicts the effect of Brownian stresses on the concentration profile at $t = 30$ (i.e., at steady-state). Particle stress hinders the rod orientations toward the flow direction in the channel. It also favors the migration of rods toward the walls as aligned rods have less tendency to migrate across the streamlines [1].

The effect of hydrodynamic stress contribution through N_p is tested. Values of N_p up to 100 show no significant modifications in the velocity profile and concentration distribution. Note that the limit of convergence of this numerical model is $N_p = 100$, for higher values the numerical model diverges.

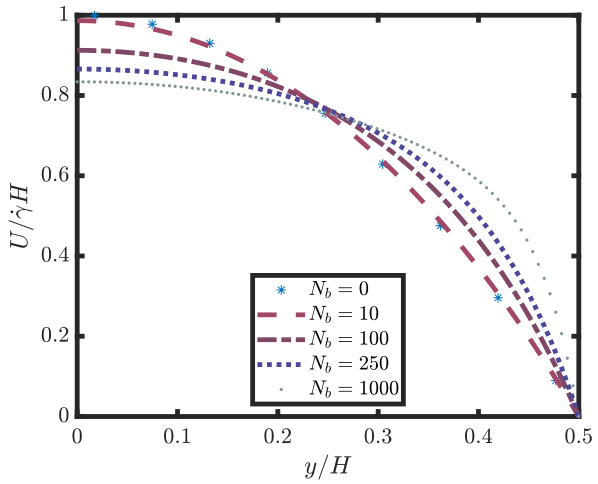

(a) Velocity profiles along the y-direction for $N_p = 0$ and for various values of N_b at $t = 30$.

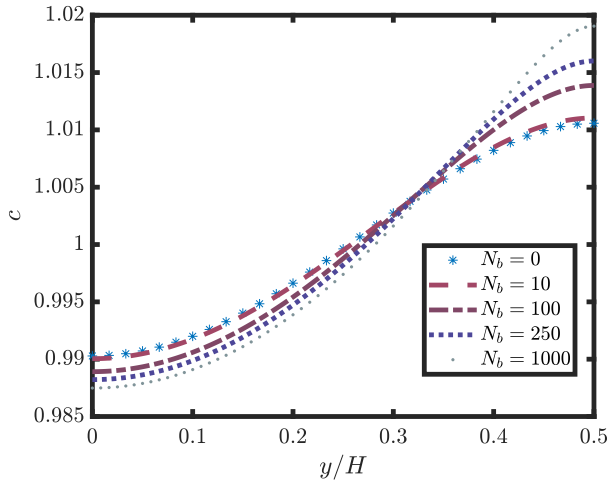

(b) Concentration distributions along the y-direction for $N_p = 0$ and for various values of N_b at $t = 30$.

FIG. 7: Effect of Brownian stress contribution on the (a) velocity profile and the (b) concentration distribution along the y-direction for $N_b = 0, 10, 100, 250$ and 1000 at $t = 30$ at $t = 30$ with $N_p = 0$.

2. *Effect of translational diffusion*

In our previous work [1], the effect of translational diffusion in a limited planar channel is studied without flow coupling. We aim now to explore the effect of translational diffusion in an infinite channel by taking into account the two-way coupling effects in a transient study. Therefore, the coupling coefficients and the rotary Peclet number are set at fixed values, such as $N_b = 250$, $N_p = 10$ and $Pe_r = 10$ with varying values of $Pe_\perp$.

Fig. 8a shows the effect of translational diffusion on the velocity profile compared with the initial velocity. It is found that extra stress has a more pronounced impact on the velocity profile at higher translational diffusion Peclet numbers.

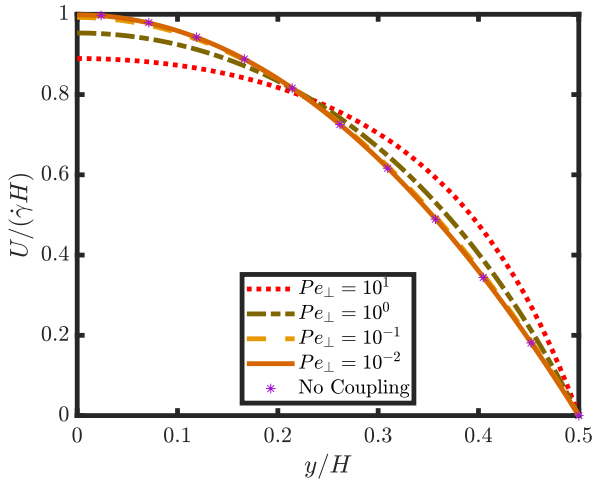

(a) Velocity profiles along the y-direction for various $Pe_\perp$ at $t = 30$ compared with velocity profile with no coupling.

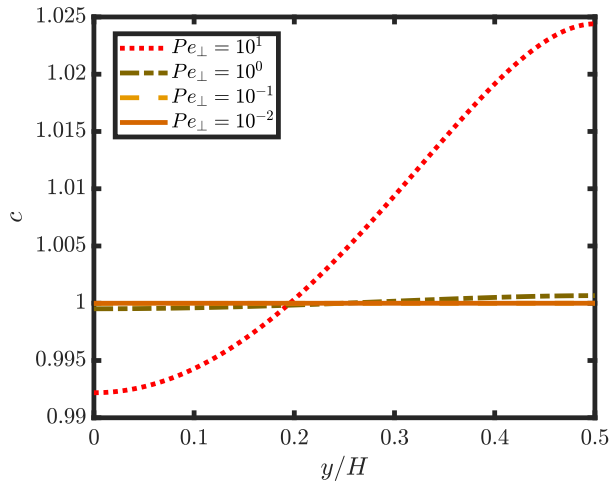

(b) Concentration along the y-direction for various $Pe_\perp$ at $t = 30$

FIG. 8: Effect of the translational Peclet number on the (a) velocity profile and the (b) concentration distribution along the y-direction for $Pe_\perp = 10^{-2}, 10^{-1}, 10^0$ and 10^1 at $t = 30$.

Fig. 8b illustrates the influence of translational diffusion on the concentration distribution of the rods. At high values of $Pe_\perp$, there is a notable migration of the rods towards the walls of the channel. However, as $Pe_\perp$ decreases, this migration becomes less pronounced. When $Pe_\perp$ drops below 10^{-1}, the rods tend to remain more uniformly distributed along the channel without significant concentration variations. In addition, the rods tend to maintain an isotropic distribution at low values of $Pe_\perp$ (results not shown). Consequently, the rheological properties of the suspension are close to the ones of the suspending fluid when $Pe_\perp$ becomes low (for more details, see Appendix B).

3. Effect of concentration gradient

A concentration gradient is now introduced keeping the rod orientation distribution isotropic. The same concentration gradient cases are considered as in Section III A 2. The numerical simulations are performed with $N_b = 250$, $N_p = 10$ and $Pe_r = Pe_\perp = 10$. No significant effect on the rod orientation is observed.

Figs. 9, 10, 11, and 12 show that the initial concentration gradients change the transient behavior of the velocity profile, shear stress and both normal stresses differences. In a suspension of Brownian rods, the shear stress and normal stress differences can undergo transient changes. These variations are caused by the presence of a concentration gradient within the suspension, which in turn affects the generation of extra stress on the fluid. However, it is crucial to emphasize that these transient changes do not impact the final steady-state values. As the rods migrate across streamlines, the concentration gradient gradually diminishes, leading the system to reach a steady state characterized by a well-developed and consistent concentration distribution. In this steady-state condition, the system achieves a stable equilibrium, with final shear stress and normal stress difference values that are the same across the channel for all the studied cases. Once the concentration becomes homogeneously distributed and the system reaches this equilibrium state, the rheological properties no longer exhibit transient changes and maintain their steady-state values throughout the channel.

C. Couette flow

The Couette flow is commonly used to study fluid dynamics and transport phenomena in cylindrical geometries. Fig. 13 shows the Couette flow geometry used in this section, which consists of two concentric cylinders with radii R_{out} and $R_{in} = 0.8R_{out}$. The outer cylinder is fixed, while the inner cylinder is rotating at angular velocity $U/(\dot{\gamma}R_{out}) = 0.36$. Fig. 13 also displays the magnitude of the velocity field between the coaxial cylinders, which varies with the radial distance. All the results in this section are plotted at the "baseline" (see Fig. 13), since at this line the velocity

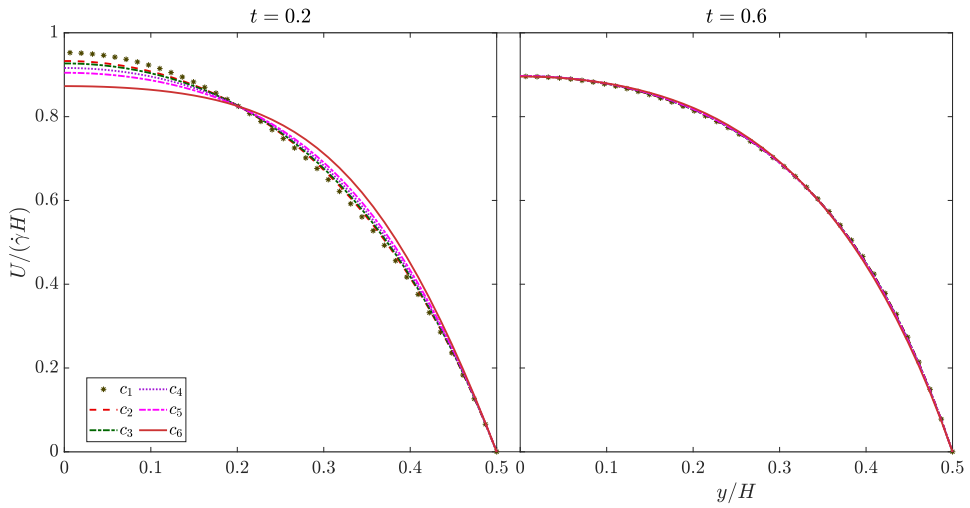

FIG. 9: Effect of the initial concentration on the velocity profile along the y-direction at $t = 0.2$, and 0.6.

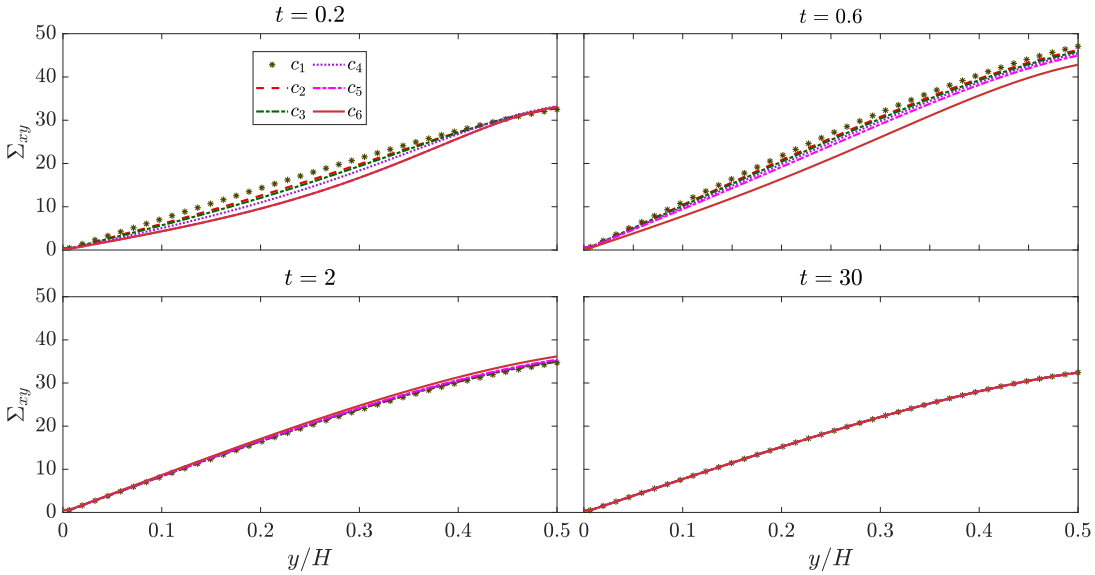

FIG. 10: Effect of the initial concentration on the shear viscosity along the y-direction at $t = 0.2, 0.6, 2$ and 30.

vector has only one component in the θ-direction. Using a cylindrical coordinate system (r, θ, z) is suitable to present the results.

1. Small gap

We first consider a flow between two concentric cylinders with a very small gap, known as Couette flow ($R_{in}/R_{out} = 0.99$). The difference in shear rates between the inner and outer cylinders is found to be around 2.8% ($\dot{\gamma} = 1 \pm 2.8\% s^{-1}$). The rotary diffusion is fixed to a value of $Pe_r = 10$ and the coupling coefficients are chosen to be $N_p = 10$ and $N_b = 250$. We observe that even a small difference in the shear rates between the inner and outer cylinders can have a significant effect on the system. The particles do not introduce any noticeable alterations to the flow field, and there is no migration of particles across the streamlines. However, the orientation of the rods in the Couette flow is influenced by the translational Peclet number, as shown in Fig. 14. The changes in particle orientation have notable consequences on the rheological properties of the system, as depicted in Fig. 15. The isotropic distribution of rods at these conditions leads to a minimal value of the shear viscosity comparable to the case of aligned rods, as well as for both normal

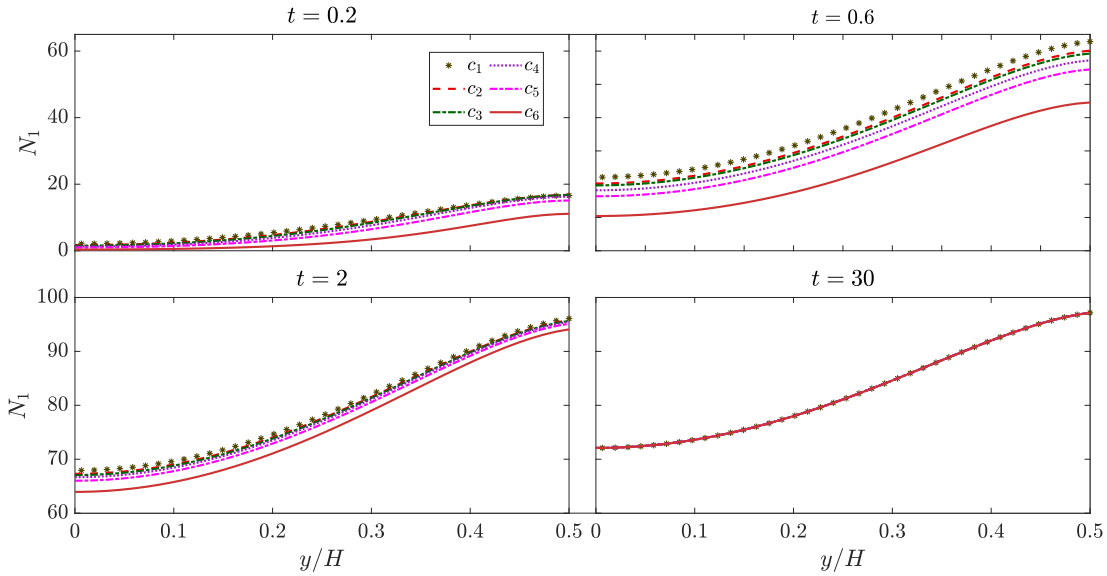

FIG. 11: Effect of the initial concentration on the first normal stress differences along the y-direction at $t = 0.2, 0.6, 2$ and 30.

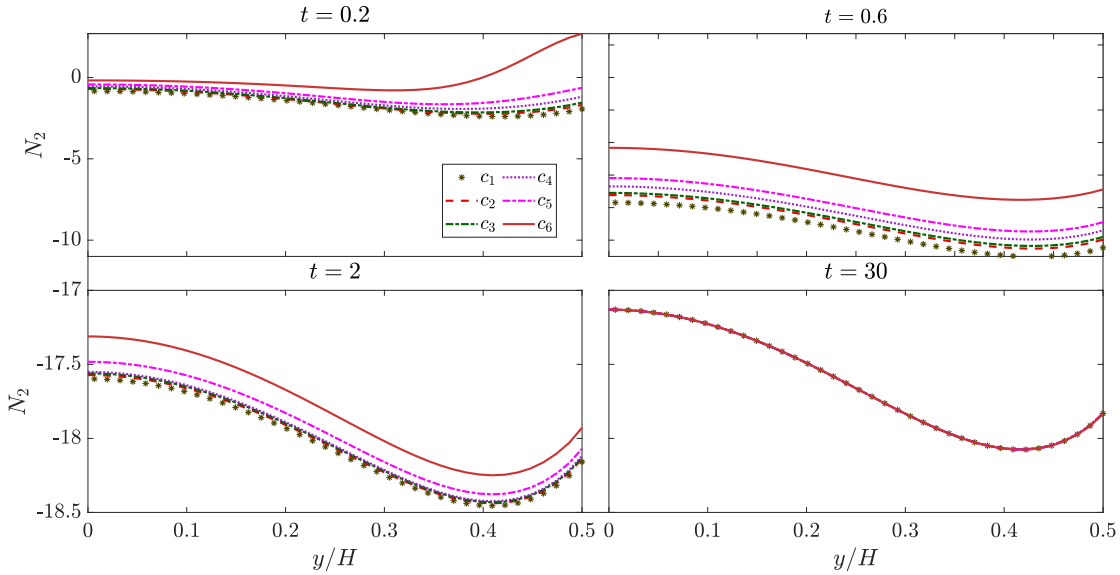

FIG. 12: Effect of the initial concentration on the second normal stress differences along the y-direction at $t = 0.2, 0.6, 2$ and 30.

stress differences. This behavior highlights the significant impact of rod orientation on the rheological properties of the suspension.

2. Effect of particle extra stresses

Fig. 16a illustrates the effect of Brownian stress contribution on the velocity profile in a Couette flow with suspended rods. It shows that as the Brownian coupling increases, the velocity profile becomes more flattened. This is because the orientation of the elongated particles affects the stress contributions, which in turn changes the shear viscosity.

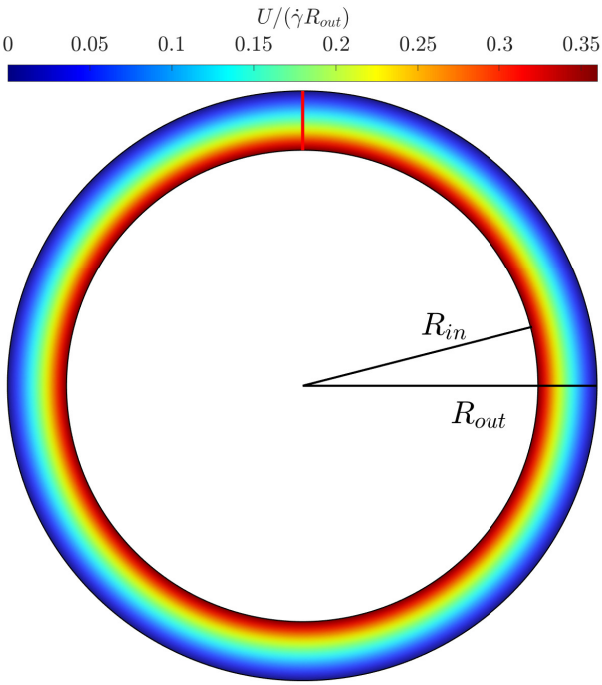

FIG. 13: Initial dimensionless velocity magnitude in the Couette flow. The red vertical line will be referred to as "the base line" in this work

As a result, the velocity profile deviates from the initial profile observed in a Couette flow

$$u_\theta/(\dot{\gamma}R_{out}) = \frac{1}{R_{out}^2 - R_{in}^2}\left(\frac{0.45R_{in}^2R_{out}}{r} - \frac{0.45R_{in}^2 r}{R_{out}}\right). \tag{20}$$

When $N_b = 100$ or 250, the coupling between the flow-field and rod orientation is strong enough to cause the formation of a reverse flow near the fixed cylinder. This occurs because the orientation of the rods affects the flow field, leading to the formation of a pressure gradient that opposes the initial flow direction (last term in Eq. (16)). As a result, the velocity near the fixed cylinder becomes negative.

Fig. 16b depicts the effect of Brownian coupling on the concentration of the rods. It indicates that as N_b increases, the concentration of rods near the fixed wall decreases and becomes more concentrated near the moving wall. This is due to the change in the velocity profile mentioned earlier.

3. Effect of translational diffusion

The effect of translational diffusion on the behavior of Brownian particles in the Couette flow is investigated by simulating the flow for various values of $Pe_\perp$. The results show that the behavior of the suspension in the Couette flow is qualitatively similar to that observed in the Poiseuille flow. Fig. 17a reports the velocity profile between the coaxial cylinders at $t = 30$. As expected, the velocity profile changes as the coupling between the particles and the flow increases. Furthermore, the effect of coupling decreases as the translational Peclet number decreases. Fig. 17b depicts the concentration distribution between the coaxial cylinders at $t = 30$. It demonstrates that at high values of $Pe_\perp$, the rods exhibit a migration towards the walls. Conversely, as $Pe_\perp$ decreases, this migration becomes less pronounced. At low values of $Pe_\perp$, the rods tend to maintain an isotropic distribution. This isotropic behavior significantly influences the rheological properties. The concentration distribution and migration of the rods play a crucial role in determining the overall rheology and behavior of the suspension in a Couette flow.

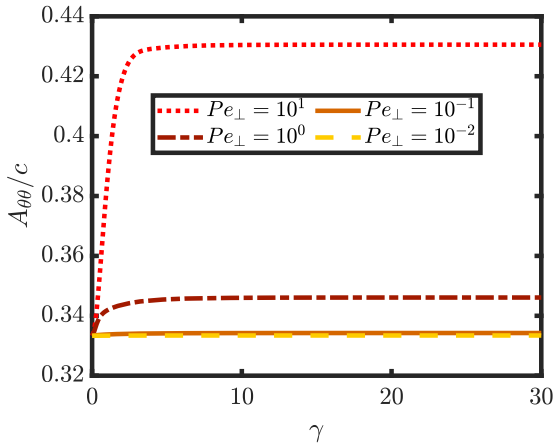

(a) Evolution of $A_{\theta\theta}$ with respect to the strain.

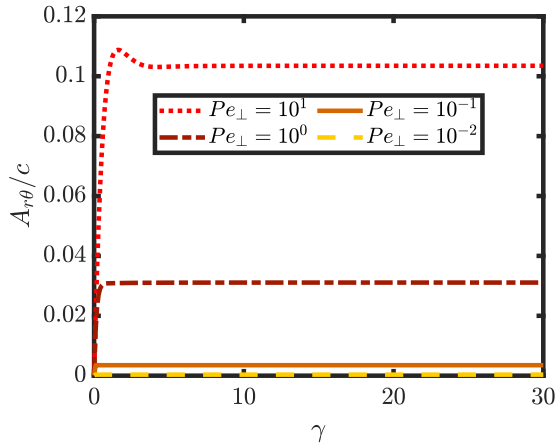

(b) Evolution of $A_{r\theta}$ with respect to the strain.

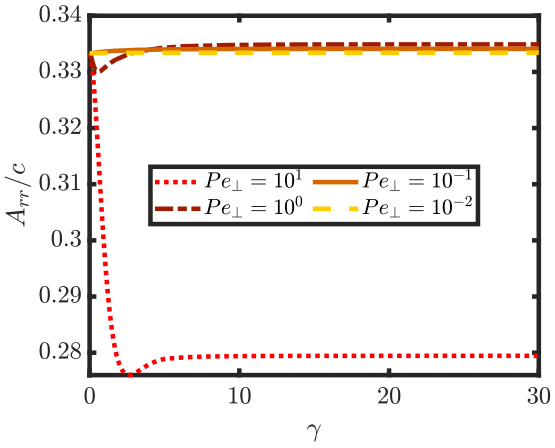

(c) Evolution of A_{rr} with respect to the strain.

FIG. 14: Effect of the translational Peclet number on the evolution of the orientation components of (a) $A_{\theta\theta}$, (b)$A_{r\theta}$ and (c) A_{rr} as a function of strain (γ) at $r = (R_{in} + R_{out})/2$ ($\dot{\gamma} = 1/s$).

IV. CONCLUSION

This numerical work investigates the rheological behavior of Brownian rod suspensions in a simple shear flow, a Poiseuille flow, and a Couette flow, respectively. The effects of rod-fluid coupling, concentration gradients, and translational diffusion are explored based on a kinetic macro-model.

The presence of rods in simple shear flow does not significantly alter the flow behavior, and translational diffusion has minimal impact on the system. However, in Poiseuille flow, the rods cause deviations from the standard parabolic velocity profile, leading to a flattened profile and the formation of concentration gradients. The coupling between the flow-field and rod orientation affects their orientation, migration behavior, and rheological properties, which have implications for the overall flow dynamics. In Couette flow, the rod-fluid coupling leads to an interesting phenomenon of inverse flow near the fixed cylinder, driven by the interplay between rod orientation and flow field.

Also, we highlight here the influence of translational Peclet numbers on the behavior of Brownian rod suspensions in flow systems. Low values of the translational Peclet number hinder the effects of rod-flow couplings, resulting in minimal alterations to the flow behavior. However, as the translational Peclet number increases, pronounced migration of rods towards the channel walls and increased alignment with the flow direction are observed. The results of our work show that the famous sentence from Doi and Edwards [10], mentioned in the introduction, is only valid for simple shear flow and even the slight deviation from linearity breaks this statement.

These results have significant implications for various applications involving rod-like particle suspensions. Under-

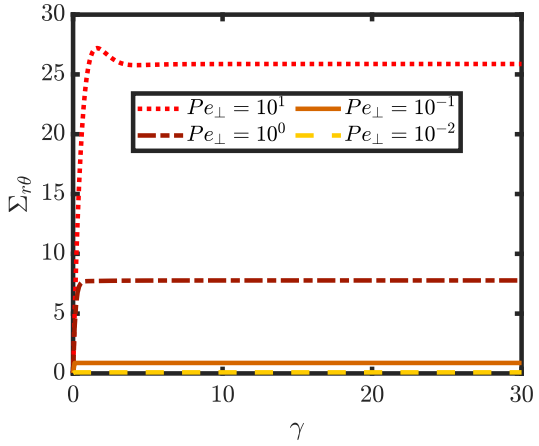

(a) Evolution of the shear viscosity ($\Sigma_{r\theta}$) with respect to the strain.

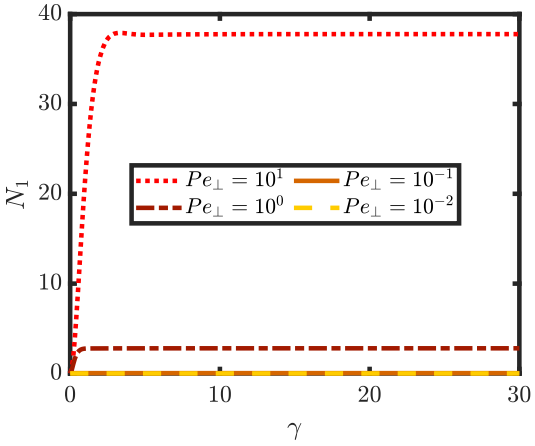

(b) Evolution of the first normal stress difference (N_1) with respect to the strain.

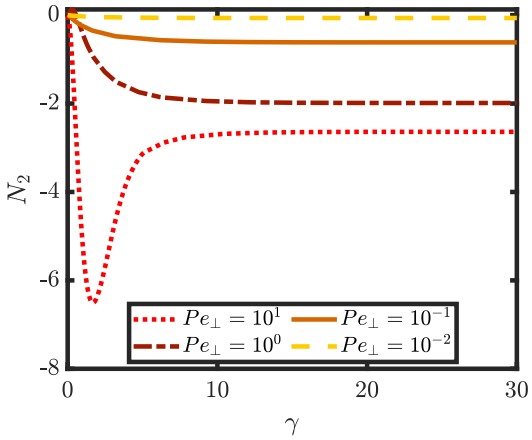

(c) Evolution of the second normal stress difference (N_2) with respect to the strain.

FIG. 15: Effect of the translational Peclet number on the evolution of the normalized rheological properties (a) shear viscosity ($\Sigma_{r\theta}$), (b) first normal stress difference (N_1) and (c) second normal stresses difference (N_2) as a function of strain (γ) at $r = (R_{in} + R_{out})/2$ ($\dot{\gamma} = 1/s$).

standing the influence of translational Peclet numbers can aid in the design and optimization of microfluidic devices, biophysical processes, and industrial applications, where the control and manipulation of rod-like particles in flow systems are crucial. Further research and experimental investigations are necessary to validate and expand upon these findings, exploring the interplay between translational diffusion and rod-flow couplings. Future works will focus on exploring the effect of anisotropic translational diffusion in the case of active Brownian particles as well as the effect of the stresses on the system.

V. ACKNOWLEDGMENTS

H.I. particularly wishes to acknowledge the Brittany Region and ISblue for their financial support. G.N. acknowledges financial support from the Natural Sciences and Engineering Research Council of Canada (NSERC) (RGPIN-03783).

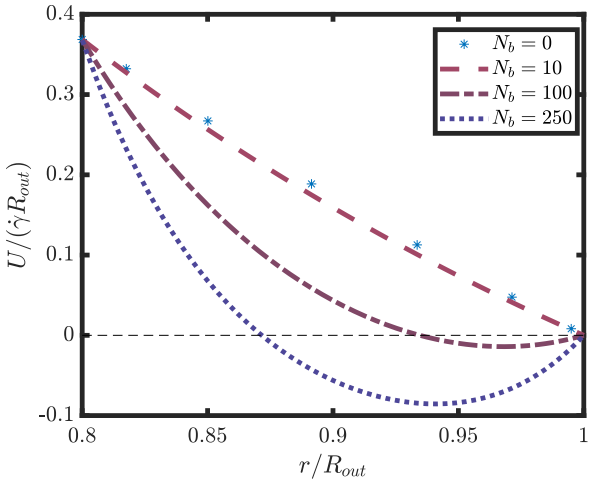

(a) Velocity profiles along the r-direction for $N_b = 0, 10, 100$ and 250 at $t = 30$.

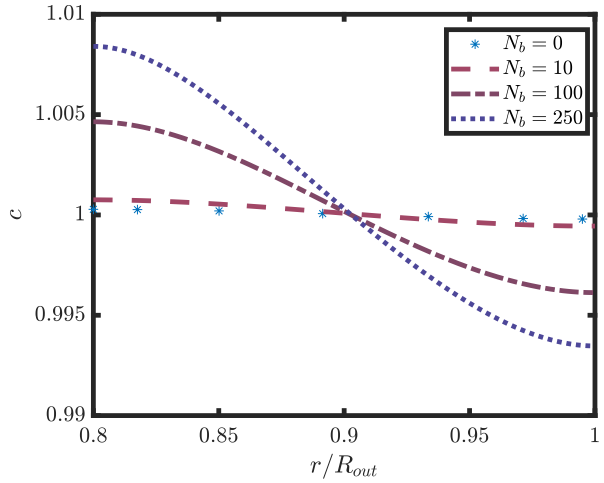

(b) Concentration distributions along the r-direction for $N_b = 0, 10, 100$ and 250 at $t = 30$.

FIG. 16: Effect of Brownian stress contribution on the (a) velocity profile and (b) concentration distribution along the r-direction for $N_b = 0, 10, 100$ and 250, and $N_p = 0$ at $t = 30$.

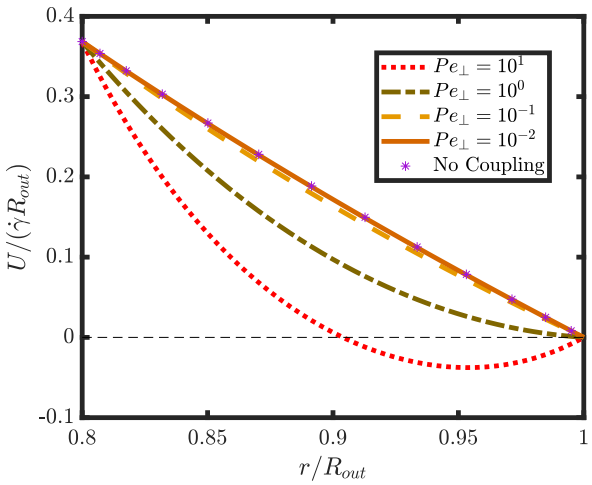

(a) Effect of the translational Peclet number on the velocity profile along the r-direction of the base line for $Pe_\perp = 10^{-2}, 10^{-1}, 10^0$ and 10^1 at $t = 30$.

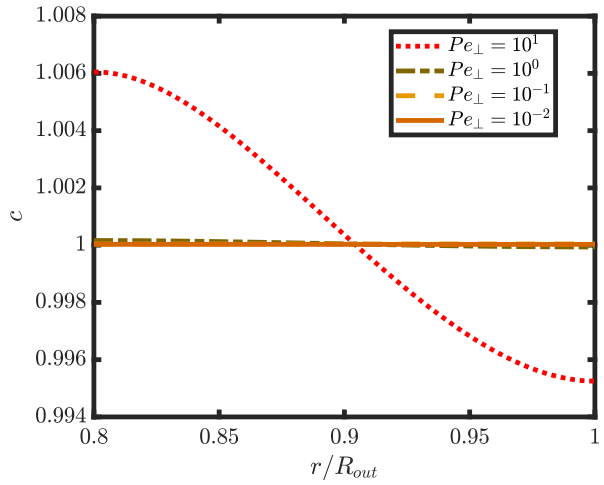

(b) Effect of the translational Peclet number on the concentration along the r-direction of the base line for $Pe_\perp = 10^{-2}, 10^{-1}, 10^0$ and 10^1 at $t = 30$.

FIG. 17: Effect of the translational Peclet number on ((a) velocity profile and (b) concentration along the r-direction for $Pe_\perp = 10^{-2}, 10^{-1}, 10^0$ and 10^1 at $t = 30$.

Appendix A: Model validation

Based on Section II C, the dimensionless form of Eq. (10) is

$$\frac{D\Psi^*}{Dt^*} = \nabla^*_{\mathbf{x}} \cdot \left\{ \left[\frac{1}{Pe_{\parallel}} \mathbf{pp} + \frac{1}{Pe_\perp} (\boldsymbol{\delta} - \mathbf{pp}) \right] \cdot \nabla^*_{\mathbf{x}} \Psi^* \right\} - \nabla_{\mathbf{p}} \cdot (\dot{\mathbf{p}}^*_j \Psi^*) + \frac{1}{Pe_r} \nabla^2_{\mathbf{p}} \Psi^*. \tag{A1}$$

In order to solve Eq. (A1) for homogeneous flows in 3D, a finite volume method is employed to discretize the partial differential equation in the configurational space. Following the works of [25] and [35], the numerical method is updated to deal with the 3D representation of Brownian particles and consists on discretizing the Fokker-Planck

equation for NxN number of equations. The model is implemented using COMSOL Multiphysics live-linked with MATLAB which uses the Finite Element (FE) method to solve the whole equations. The two-way coupling of fluid and particles is taken into account using the weak formulation of the equations in the laminar flow physics interface. The study of the numerical solution of the model is performed to verify the used model in a simple shear flow. We compare the results with published data in the case of a homogeneous system by performing single-point calculations (SPC) using the finite volume method. SPC calculation is performed by discretizing the half sphere of the unit radius into $N = 120$x120 area elements, whereas only $N = 20$x20 element areas are considered for the FE scheme. Starting from the initially homogeneous concentration $c(t = 0) = 1$ and the initially isotropic orientation of the particles, the orientation state is expressed as a function of total strain in Fig. 18. A_{11} and A_{22} are proportional to the magnitude of the alignment in the flow direction and velocity gradient direction, respectively, while A_{12} indicates the direction of alignment. The model is simulated for $Pe_r = 10$, $Pe_\perp = 10^9$ (which has no physical effect on translational diffusion except for stabilizing the numerical scheme) in a transient study for $\gamma = 30$ without considering the hydrodynamic and Brownian coupling effects. The concentration remains homogeneous ($c = 1$) during the study. Fig. 18 illustrates a comparison between SPC and FE results, and using the IBOF closure. The FE results and the model using the IBOF closure provide accurate dynamics and the appropriate steady-state values. This analysis confirms the well-implementation of the FE code and the IBOF accuracy in this work.

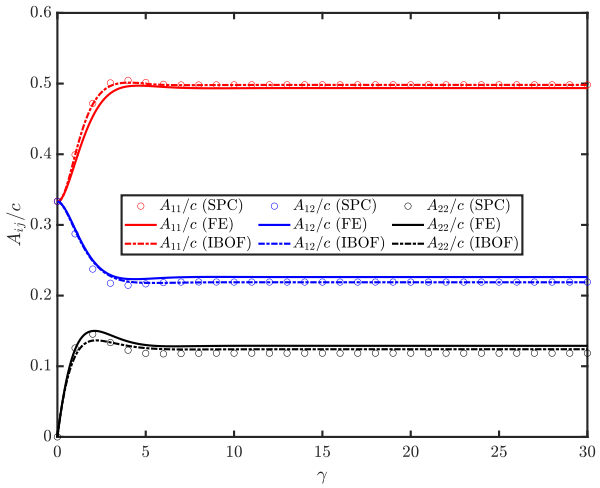

FIG. 18: Comparison of the IBOF closure approximation [26] with the FE and single-point calculations (SPC) of the conformation tensor components in simple shear flow ($\dot{\gamma} = 1$) with respect to strain γ.

Appendix B: Effect of translational diffusion on the rheological transient behaviors in Poiseuille flow

Fig. 19 shows the evolution of the shear stress profile along the y-direction for the mentioned time steps at various $Pe_\perp$ numbers. The results indicate that the shear stress Σ_{xy} of the suspension is highest near the walls, where the shear stress and the alignment of the particles are highest, and lowest at the center of the channel, where the shear stress and the alignment of the particles are lowest. As $Pe_\perp$ increases, Σ_{xy} increases.

Figs. 20 and 21 present the normal stress differences for the mentioned translational Peclet numbers at the same time steps. Due to the higher rod alignment at higher translational Peclet numbers, first normal stress differences increase with the increase of $Pe_\perp$. For $Pe_\perp = 10^{-1}$ and 10^{-2}, N_1 values are around zero. N_2 exhibits negative values, it has higher values around the center of the channel than near the walls. As time increases, N_2 decreases until it reaches the steady state. Increasing $Pe_\perp$ leads to lower values of N_2, at low $Pe_\perp$, N_2 remains around zero. Due to the anisotropic nature of the suspension, normal stress differences develop. The particles initially take some time to align and arrange themselves in the flow direction after the flow is initiated.

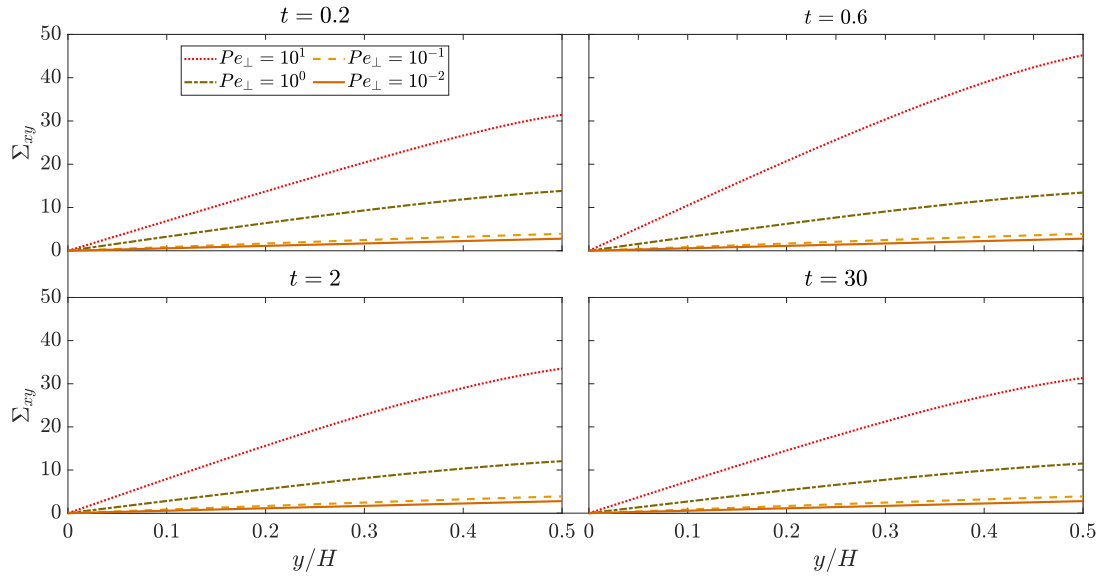

FIG. 19: Effect of the translational Peclet number on the shear stress Σ_{xy} along the y-direction for various $Pe_\perp$ numbers at different time t.

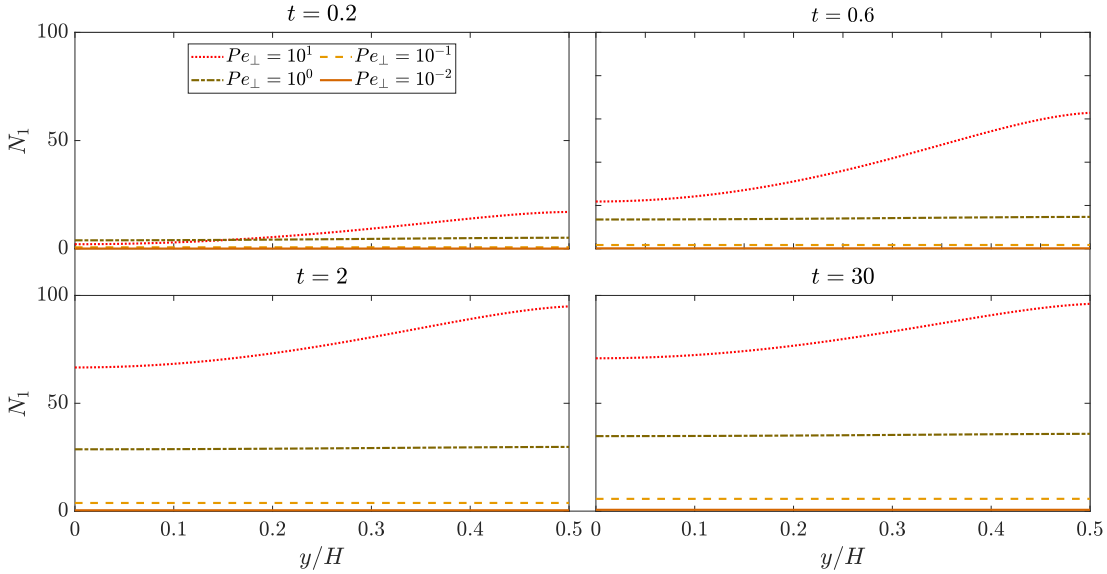

FIG. 20: Effect of the translational Peclet number on the first normal stress difference N_1 along the y-direction for various $Pe_\perp$ numbers at different time t.

[1] H. Issa, G. Natale, G. Ausias, and J. Férec, Modeling and numerical simulations of Brownian rodlike particles with anisotropic translational diffusion, Phys. Rev. Fluids **8**, 033302 (2023).

[2] J. Thomason and W. Groenewoud, The influence of fibre length and concentration on the properties of glass fibre reinforced polypropylene: 2. Thermal properties, Composites Part A: Applied Science and Manufacturing **27**, 555 (1996).

[3] S. Houshyar, R. Shanks, and A. Hodzic, The effect of fiber concentration on mechanical and thermal properties of fiber-reinforced polypropylene composites, Journal of applied polymer science **96**, 2260 (2005).

[4] M. Li, Z. Ali, X. Wei, L. Li, G. Song, X. Hou, H. Do, J. C. Greer, Z. Pan, C.-T. Lin, N. Jiang, and J. Yu, Stress induced carbon fiber orientation for enhanced thermal conductivity of epoxy composites, Composites Part B **208**, 108599 (2021).

[5] W. Russel, Brownian motion of small particles suspended in liquids, Annual Review of Fluid Mechanics **13**, 425 (1981).

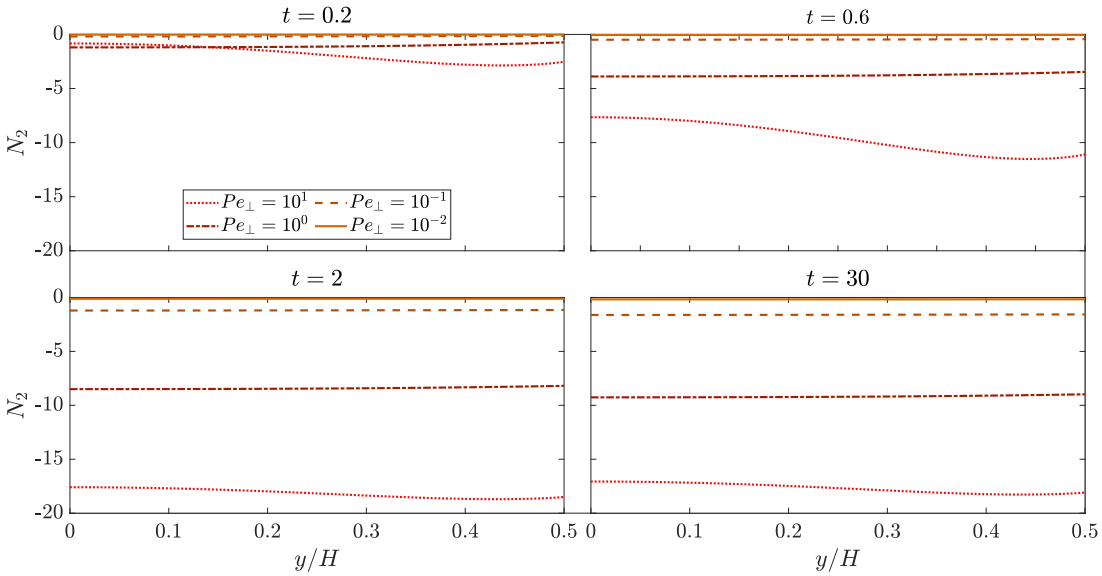

FIG. 21: Effect of the translational Peclet number on the second normal stress difference N_2 along the y-direction for various $Pe_\perp$ numbers at different time t.

[6] A. Ladd and R. Verberg, Lattice-boltzmann simulations of particle-fluid suspensions, Journal of statistical physics **104**, 1191 (2001).

[7] G. B. Jeffery, The motion of ellipsoidal particles immersed in a viscous fluid, Proceedings of the Royal Society of London. Series A, Containing papers of a mathematical and physical character **102**, 161 (1922).

[8] C. A. Stover, D. L. Koch, and C. Cohen, Observations of fibre orientation in simple shear flow of semi-dilute suspensions, Journal of Fluid Mechanics **238**, 277 (1992).

[9] M. Rahnama, D. L. Koch, Y. Iso, and C. Cohen, Hydrodynamic, translational diffusion in fiber suspensions subject to simple shear flow, Physics of Fluids A: Fluid Dynamics **5**, 849 (1993).

[10] M. Doi and S. Edwards, *The theory of polymer dynamics*, Vol. 73 (Oxford university press, 1988).

[11] J. K. Dhont and W. J. Briels, Rod-like Brownian particles in shear flow, Soft Matter: Complex Colloidal Suspensions, edited by G. Gompper, M. Schick **2** (2006).

[12] J. Férec, G. Ausias, M. Heuzey, and P. Carreau, Modeling fiber interactions in semiconcentrated fiber suspensions, Journal of Rheology **53**, 49 (2009).

[13] G. Natale, M. Heuzey, P. Carreau, G. Ausias, and J. Férec, Rheological modeling of carbon nanotube suspensions with rod–rod interactions, AIChE Journal **60**, 1476 (2014).

[14] E. Hinch and L. Leal, Time-dependent shear flows of a suspension of particles with weak Brownian rotations, Journal of Fluid Mechanics **57**, 753 (1973).

[15] A. Hijazi and M. Zoaeter, Brownian dynamics simulations for rod-like particles in dilute flowing solution, European polymer journal **38**, 2207 (2002).

[16] B. D. Leahy, D. L. Koch, and I. Cohen, The effect of shear flow on the rotational diffusion of a single axisymmetric particle, Journal of Fluid Mechanics **772**, 42 (2015).

[17] D. Palanisamy and W. K. den Otter, Efficient Brownian dynamics of rigid colloids in linear flow fields based on the grand mobility matrix, The Journal of Chemical Physics **148**, 194112 (2018).

[18] R. L. Schiek and E. S. Shaqfeh, Cross-streamline migration of slender Brownian fibres in plane poiseuille flow, Journal of Fluid Mechanics **332**, 23 (1997).

[19] L. C. Nitsche and E. Hinch, Shear-induced lateral migration of Brownian rigid rods in parabolic channel flow, Journal of Fluid Mechanics **332**, 1 (1997).

[20] D. Xie, M. Lista, G. G. Qiao, and D. E. Dunstan, Shear induced alignment of low aspect ratio gold nanorods in Newtonian fluids, The Journal of Physical Chemistry Letters **6**, 3815 (2015).

[21] G. Kumar and G. Natale, Settling dynamics of two spheres in a suspension of Brownian rods, Physics of Fluids **31**, 073104 (2019).

[22] S. G. Advani and C. L. Tucker III, The use of tensors to describe and predict fiber orientation in short fiber composites, Journal of rheology **31**, 751 (1987).

[23] R. J. Phillips, R. C. Armstrong, R. A. Brown, A. L. Graham, and J. R. Abbott, A constitutive equation for concentrated suspensions that accounts for shear-induced particle migration, Physics of Fluids A: Fluid Dynamics **4**, 30 (1992).

[24] N. C. Shapley, R. C. Armstrong, and R. A. Brown, Laser doppler velocimetry measurements of particle velocity fluctuations in a concentrated suspension, Journal of Rheology **46**, 241 (2002).

[25] J. Férec, M. Heniche, M. Heuzey, G. Ausias, and P. Carreau, Numerical solution of the Fokker-Planck equation for fiber suspensions: application to the Folgar–Tucker–Lipscomb model, Journal of non-Newtonian fluid mechanics **155**, 20 (2008).
[26] D. H. Chung and T. H. Kwon, Invariant-based optimal fitting closure approximation for the numerical prediction of flow-induced fiber orientation, Journal of rheology **46**, 169 (2002).
[27] D. Saintillan and M. J. Shelley, Active suspensions and their nonlinear models, Comptes Rendus Physique **14**, 10.1016/j.crhy.2013.04.001 (2013).
[28] S. Weady, M. J. Shelley, and D. B. Stein, A fast chebyshev method for the Bingham closure with application to active nematic suspensions, Journal of Computational Physics **457**, 110937 (2022).
[29] G. Batchelor, The stress system in a suspension of force-free particles, Journal of fluid mechanics **41**, 545 (1970).
[30] G. Batchelor and J. Green, The determination of the bulk stress in a suspension of spherical particles to order c2, Journal of Fluid Mechanics **56**, 401 (1972).
[31] G. Batchelor, The effect of Brownian motion on the bulk stress in a suspension of spherical particles, Journal of fluid mechanics **83**, 97 (1977).
[32] R. A. Bagnold, Experiments on a gravity-free dispersion of large solid spheres in a Newtonian fluid under shear, Proceedings of the Royal Society of London. Series A. Mathematical and Physical Sciences **225**, 49 (1954).
[33] F. A. Gadala-Maria, *The rheology of concentrated suspensions.* (Stanford University, 1979).
[34] F. Gadala-Maria and A. Acrivos, Shear-induced structure in a concentrated suspension of solid spheres, Journal of Rheology **24**, 799 (1980).
[35] D. Mezi, G. Ausias, S. G. Advani, and J. Férec, Fiber suspension in 2D nonhomogeneous flow: The effects of flow/fiber coupling for Newtonian and power-law suspending fluids, Journal of Rheology **63**, 405 (2019).
[36] D. Mezi, G. Ausias, Y. Grohens, and J. Férec, Numerical simulation and modeling of the die swell for fiber suspension flows, Journal of Non-Newtonian Fluid Mechanics **274**, 104205 (2019).
[37] K. Yasuda, N. Ohara, and M. Muguruma, Velocity profiles of suspension flows through an abrupt contraction measured by magnetic resonance imaging, Chemical Engineering & Technology: Industrial Chemistry-Plant Equipment-Process Engineering-Biotechnology **30**, 1036 (2007).
[38] S. Mazahir, G. Vélez-García, P. Wapperom, and D. Baird, Evolution of fibre orientation in radial direction in a center-gated disk: Experiments and simulation, Composites Part A: Applied Science and Manufacturing **51**, 108 (2013).
[39] S. Mazahir, G. Vélez-García, P. Wapperom, and D. Baird, Fiber orientation in the frontal region of a center-gated disk: Experiments and simulation, Journal of Non-Newtonian Fluid Mechanics **216**, 31 (2015).
[40] J. Wang, J. F. O'Gara, and C. L. Tucker III, An objective model for slow orientation kinetics in concentrated fiber suspensions: Theory and rheological evidence, Journal of Rheology **52**, 1179 (2008).
[41] A. Moosaie and M. Manhart, A direct numerical simulation method for flow of Brownian fiber suspensions in complex geometries, Journal of dispersion science and technology **34**, 427 (2013).
[42] P. J. Krochak, J. A. Olson, and D. M. Martinez, Fiber suspension flow in a tapered channel: The effect of flow/fiber coupling, International journal of multiphase flow **35**, 676 (2009).
[43] S. G. Advani and C. L. Tucker III, Closure approximations for three-dimensional structure tensors, Journal of Rheology **34**, (1990).
[44] J. S. Cintra Jr and C. L. Tucker III, Orthotropic closure approximations for flow-induced fiber orientation, Journal of Rheology **39**, 1095 (1995).